Characterizing water surface elevation under different flow conditions for the upcoming SWOT mission

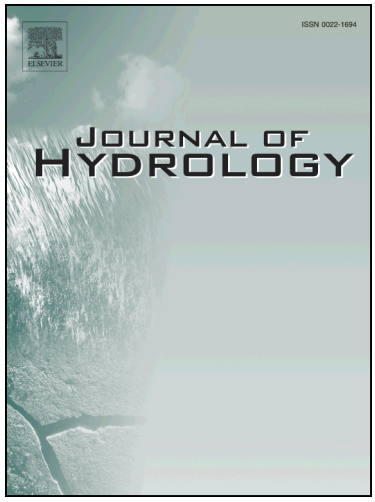

Research papers

Characterizing water surface elevation under different flow conditions for the upcoming SWOT mission

A. Domeneghetti, G. Schumann, R.P.M. Frasson, R. Wei, T. Pavelsky, A. Castellarin, A. Brath, M. Durand

PII: S0022-1694(18)30299-3
DOI: https://doi.org/10.1016/j.jhydrol.2018.04.046
Reference: HYDROL 22749

To appear in: *Journal of Hydrology*

Received Date: 3 August 2017
Revised Date: 17 April 2018
Accepted Date: 18 April 2018

Please cite this article as: Domeneghetti, A., Schumann, G., Frasson, R.P.M., Wei, R., Pavelsky, T., Castellarin, A., Brath, A., Durand, M., Characterizing water surface elevation under different flow conditions for the upcoming SWOT mission, *Journal of Hydrology* (2018), doi: https://doi.org/10.1016/j.jhydrol.2018.04.046

Characterizing water surface elevation under different flow conditions for the upcoming SWOT mission

A. Domeneghetti*[1], G. Schumann[2,3], R. P.M. Frasson[4], R. Wei[4], T. Pavelsky[5], A. Castellarin[1], A. Brath[1], M. Durand[6]

*corresponding Author: alessio.domeneghetti@unibo.it

[1] DICAM, School of Engineering, Bologna, Italy

[2] Remote Sensing Solutions Inc., Monrovia, California, United States

[3] School of Geographical Sciences, University of Bristol, Bristol, United Kingdom

[4] Byrd Polar and Climate Research Center, The Ohio State University, Columbus, United States

[5] Department of Geological Sciences, University of North Carolina, Chapel Hill, United States

[6] School of Earth Sciences, The Ohio State University, Columbus, United States

HIGHLIGHTS

1) Evaluation of SWOT-like data under different flow conditions: high, low and mean flow

2) Simulations show high performance of SWOT in sensing water surface elevation (-0.21 m)

3) Water height errors for the high flow scenario are lower than in other flow conditions

4) River orientation, topography and cross-track distance affect performance

ABSTRACT

The Surface Water and Ocean Topography satellite mission (SWOT), scheduled for launch in 2021, will deliver two-dimensional observations of water surface heights for lakes, rivers wider than 100 m and oceans. Even though the scientific literature has highlighted several fields of application for the expected products, detailed simulations of the SWOT radar performance for a realistic river scenario have not been presented in the literature. Understanding the error of the most fundamental "raw" SWOT hydrology product is important in order to have a greater awareness about strengths and limits of the forthcoming satellite observations. This study focuses on a reach (~140 km in length) of the middle-lower portion of the Po River, in Northern Italy, and, to date, represents one of the few real-case analyses of the spatial patterns in water surface elevation accuracy expected from SWOT. The river stretch is characterized by a main channel varying from 100-500 m in width and a large floodplain (up to 5 km) delimited by a system of major embankments. The simulation of the water surface along the Po River for different flow conditions (high, low and mean annual flows) is performed with inputs from a quasi-2D model implemented using detailed topographic and bathymetric information (LiDAR, 2 m resolution). By employing a simulator that mimics many SWOT satellite sensor characteristics and generates proxies of the remotely sensed hydrometric data, this study characterizes the spatial observations potentially provided by SWOT. We evaluate SWOT performance under different hydraulic conditions and assess possible effects of river embankments, river width, river topography and distance from the satellite ground track. Despite analyzing errors from the raw radar pixel cloud, which receives minimal processing, the present study highlights the promising potential of this Ka-band interferometer for measuring water surface elevations, with mean elevation errors of 0.1 cm and 21 cm for high and low flows, respectively. Results of the study characterize the expected performance of the upcoming SWOT mission and provide additional insights into potential applications of SWOT observations.

KEYWORDS

SWOT simulator; remote sensing; Ka-band interferometer; inland water surfaces; river monitoring; Po river

1 Introduction

The monitoring of fresh water in rivers and lakes is fundamental for a large variety of scientific, societal and economic reasons. Neglecting water fluxes, the globally available freshwater represents a very small portion (3%) of the water on Earth. Of this, only 1.8% is available as superficial freshwater and directly exploitable for human needs (i.e. lakes and rivers), while the remaining part is locked in ice caps and glaciers (~68%) or in groundwater (~30%) (Prakash and Singh, 2016). Despite this limited amount and the essential role of surficial freshwater for humans and ecosystem services, its monitoring is still an open issue. In most countries, it is relatively sparsely monitored by means of ground-based stations, which measure the water surface height (referenced to some local datum) and estimate the river flows by means of rating curves. The result is a largely incomplete knowledge of river fluxes, with measurements provided by stream gauge networks of different density, accuracy and reliability over the globe (Biancamaria *et al.*, 2010; Pavelsky *et al.*, 2014; Wilson *et al.*, 2015; Pena-Arancibia *et al.*, 2015; Tomkins, 2014; Domeneghetti *et al.*, 2012). The installation and maintenance costs required to sustain the monitoring networks constrain their installation mostly to highly-developed areas. For instance, the number of gauge locations in Europe and North America is nearly 50% of the overall number of stations available through the Global Runoff Data Centre (GRDC; 2016 dataset), yet rivers in these continents only account for about 24% of the global runoff (Prakash and Singh, 2016). However, Central and South America have only 8% of the total number of gauging stations, compared to an amount of runoff that covers nearly the 25% of Earth's freshwater flows (Prakash and Singh, 2016; Shiklomanov and Rodda, 2003). In addition, when available, observation time series often suffer from data gaps, as well as national data sharing policies, or political conflicts in the case of trans-boundary basins, which may further limit the availability and use of streamflow data (Gleason & Hamdan, 2015; Hossain *et al.*, 2014; Sneddon & Fox, 2012; Vörösmarty *et al.*, 2001; Wolf *et al.*, 1999).

Although satellite data will probably never replace traditional ground-based gauges, remote sensing represents a valuable supplementary source of earth observation that is able to provide useful information for hydrological analysis and for river monitoring (e.g., Smith, 1997; Alsdorf *et al.*, 2007; Smith and Pavelsky, 2008; Durand *et al.*, 2008; Michailovsky *et al.*, 2013; Tourian *et al.*, 2013; Andreadis and Schumann, 2014; Singh and Gupta, 2016; Schumann and Domeneghetti, 2016). In particular, satellite altimetry (e.g., ENVISAT, ERS, TOPEX/Poseidon, JASON 1 and 2) has been extensively used for the monitoring of river

and lakes (see e.g., Domeneghetti *et al.*, 2014, 2015b; Jarihani *et al.*, 2015), and for the estimation of river discharge (see e.g.; Birkinshaw *et al.*, 2010; Getirana, 2010; Michailovsky *et al.*, 2013; Tarpanelli *et al.*, 2013; Tourian *et al.*, 2016). Despite the undeniable potential, the design of current satellite missions constrains the utility of such data: wide footprint resolution (from a few hundred to thousands of meters), limited ground track spatial resolution (in some cases as low as a few kilometers) and low revisit time (from 10 to 35 days) represent the main limiting factors for current satellite data. In addition, these instruments provide only a single variable at a time (i.e., water elevation, width, etc.) among those required for a proper estimation of river flows and require appropriate calibration based on ground-based data (Pavelsky *et al.*, 2014).

The forthcoming SWOT (Surface Water and Ocean Topography) mission (to be launched in 2021; https://swot.jpl.nasa.gov/) aims to overcome these limitations by providing two-dimensional and simultaneous observations of water surface elevation and water extent of inland water bodies (Durand *et al.*, 2010; Biancamaria *et al.*, 2016).

SWOT is the first surface water hydrology-dedicated satellite mission, jointly developed by NASA and CNES (the French space agency), in partnership with CSA and UKSA (Canadian and UK Space Agency, respectively). In addition to observing the ocean, SWOT is required to observe inland water bodies larger than 250 m x 250 m, with a goal of 10,000 m^2, and rivers wider than 100 m. Although not considered a baseline mission requirement, the SWOT mission has a stated goal of observing rivers wider than 50 m and water bodies as small as 1 ha (see Biancamaria *et al.*, 2016, for more details). SWOT will likely be able to produce groundbreaking results in many hydrological fields since it is expected to provide water extent, slope and water surface elevation for nearly 60% of basins larger than 50,000 km^2 (Pavelsky *et al.*, 2014). The Ka-band interferometer mounted on the satellite will ensure a spatially continuous two-dimensional observation of water elevation and inundation extent of water bodies located inside each of its two 50 km-wide swaths.

The SWOT product delivered to the end users will be the results of a post-processing averaging procedure over multiple raw pixels in order to minimize the effect of noise. The characteristics of these products, as well as the spatial resolution of river reaches to consider in order to ensure the best accuracy and effectiveness of these products, are still under study (Biancamaria *et al.*, 2016; Frasson *et al.*, 2017).

Furthermore, since lower-level products will be provided on demand, future improvements to post-processing procedures may help to achieve the goal of observing narrower rivers or smaller water bodies (Biancamaria *et al.*, 2016).

Table 1 summarizes the main science requirements of the mission (see e.g., Rodriguez, 2015; Biancamaria *et al.*, 2016) and reports the expected accuracies for the satellite observables.

Table 1. Main SWOT products requirements and goals (Rodriguez, 2015)

Variable	Condition	Requirement
Height accuracy	Averaging area > 1 km^2 62.500 m^2 < Averaging area< 1 km^2	< 10 cm < 25 cm
Slope accuracy	for a 10 km length of a 100 m wide river	1.7 cm/km
Relative errors on water extents	Water bodies > 10.000 m^2 – rivers width >50 m Water bodies > 62.500 m^2 – rivers width >100 m	< 25% < 15%

Biancamaria *et al.* (2015) have recently provided a clear and comprehensive overview of the hydrological applications that may benefit from SWOT's observations. Most of the reported usages refer to satellite observables for the monitoring of lakes and reservoirs (e.g., Biancamaria *et al.*, 2010), and for the characterization of river discharge (e.g., Durand *et al.*, 2016, and references therein). However, other possible applications include the study of transboundary river management, estuaries, ice sheet topography and snow cover. Thus, the interest of the scientific community in SWOT products is high and so the analysis and understanding of the expected observation quality is important to its scientific applicability.

In the majority of existing studies about SWOT mission potential, satellite observations are synthetically reproduced by corrupting appropriate observed or simulated data with random errors defined according to the science requirements (see Table 1; e.g., Wilson *et al.*, 2015; Durand *et al.*, 2008; Andreadis *et al.*, 2007). This appears justified by the fact that these studies are mainly aimed at testing the suitability of SWOT data for different applications (i.e., water resources management, discharge estimation, etc.) using synthetic satellite data as a proxy with a given uncertainty, constant in space and time. Even though this approach may be reasonable in absence of real remotely sensed data, it may introduce some simplifications on estimating the expected SWOT products, neglecting for example possible inaccuracies related to the real river and floodplain topography, river orientation, layover effects, distance of the target to the satellite orbit, etc.

Bonnema *et al.* (2016) and Solander *et al.* (2016) tried to overcome this limitation by using SWOT observations from a satellite simulator developed at Caltech/NASA's JPL (Jet Propulsion Laboratory) that mimics the instrument performance under real conditions (additional details on this are provided in Section 3.3). These recent studies provide useful considerations regarding satellite potential on discharge estimation (Bonnena *et al.*, 2016) and reservoir observation (Solander et a., 2016), but granting limited attention to the underlying characteristics of the data used. Frasson *et al.* (2017) have recently run the SWOT simulator over the Sacramento and the Po rivers, investigating the impact of different river-reach definition strategies on the estimation of reach-averaged hydrological variables (i.e. water height, width, slope and discharge). Although authors recognized the relevance of a possible interaction between the radar signal and the river surrounding topography (more details on that are provided in Section 3.3), performances and errors of simulator products are evaluated in terms of reach-averaged variables, and not at the detail of the most fundamental SWOT hydrology products. Therefore, further analyses are needed for a more comprehensive understanding of the value, potential and limitations of SWOT observations under actual/real conditions. This study investigates SWOT river observations and provides additional insights in relation to a real river topology under different flow conditions.

In particular, it represents one of the few analyses to date in which the simulated water heights have error characteristics similar to those expected from SWOT, as produced by the SWOT hydrology simulator, and it complements the recent SWOT hydrology literature by studying different flow conditions (i.e., high, low and mean annual flow), which cover a possible range of water extents that may occur along the study area. In particular, the application of the SWOT simulator with very detailed topographic data and a river reach representative of actual mission measurement requirements enables: (i) the investigation of potential effects of near-river topography and river orientation, and their impact on topographic layover and water height measurements expected from SWOT; (ii) the evaluation of satellite instrument performance on water height observations relative to the distance from the satellite nadir track. These objectives provide the structural sub-headings used in the following Methods (see Section 4), Results and Discussions (see Section 5) sections.

Although this study does not reflect work on actual targeted mission product requirements (characteristics of the final SWOT products are still under definition; see e.g. Biancamaria *et al.*, 2016; Frasson *et al.*, 2017),

simulations and analyses performed will contribute to ongoing discussions regarding the definition of SWOT products, as part of ongoing science team projects before and after launch.

2 Study area and available data

Figure 1 introduces the study area considered for the analysis. The Po river is the largest river in Italy, with an overall basin of about 70 090 km^2. It flows from West to East, crossing the Northern part of the country, with a total length of nearly 652 km. From the source (i.e. Mount Monviso, c.a. 2100 m above sea level (a.s.l.)) to the beginning of the river delta, in proximity of the Adriatic Sea, the Po river receives more than 141 tributaries from the Apennines (Northern side) and the close Western and Southern sides of the Alps (Montanari *et al.*, 2016). Along its course, it evolves from a typical alpine behavior to a single-channel river, passing through river reaches characterized by a braided bed, and winding course with scroll-bars and abandoned meanders. The red box in Figure 1 highlights the river reach of interest: the lower portion of the Po river (nearly 140 km), from the gauging station of Borgoforte to the beginning to the delta (see also Figure 2 for details). At this stage, the Po river has received the majority of its tributaries (conventionally the catchment outlet is the gauging station of Pontelagoscuro) and is characterized by a stable main channel, surrounded by large dike-protected floodplains, and constrained by a well-maintained embankment system.

Flow conditions vary significantly from flood to drought seasons. Even though the wet section width may reach 2470 m in case of a flood event (the Po river reaches its widest extent in this portion), the wetted area may decrease to approximately 100 m during low flow periods. Table 2 summarizes morphological features that characterize the river portion, from which emerge a notable variability of cross sectional width in relation to flows (see also Table 3).

The significance of the embankment system delimiting the river course is reflected by the overall cross-section flow depth (i.e. the difference between embankment elevation and river thalweg), on average equal to 18.8 m (see Table 2), and the embankment height over the floodplain, in some cases higher than 12 m. Those latter values highlight a peculiarity of the study area, that is the presence of high, well maintained embankments that are in some cases very close to the main channel. These conditions may represent a critical issue for remote monitoring (more details on this are reported in Section 3.3). In the light of its dimensions, hydrological regime and flow direction (perpendicular to satellite track), the Po river represents

an excellent test-case candidate for the upcoming SWOT mission. Because of the strong human impact on its morphology, the Po river might not be representative of more natural rivers where the water dynamics may differ significantly under high and low flows; however, the Po river does offer the opportunity to study the effect of embankments and other engineering features (such as storage areas) on the accuracy of the expected products.

Table 2. Morphological features of the lowest portion of the Po river (red box in Figure 1); data into brackets specify the range of variability: max-min values, respectively.

Characteristics	***Po river Borgoforte- Pontelagoscuro***
Average cross-section width (m)	890 (2485 - 360)
Average main channel width (m)	425 (850 - 159)
Average main channel depth (m)	12.8 (19.7 - 5.5)
Average embankment height over floodplain (m)	6.9 (12.8 - 4.4)
Average embankment height over river thalweg (m)	18.8 (25.2 – 11.2)
Sinuosity index (-)	1.23

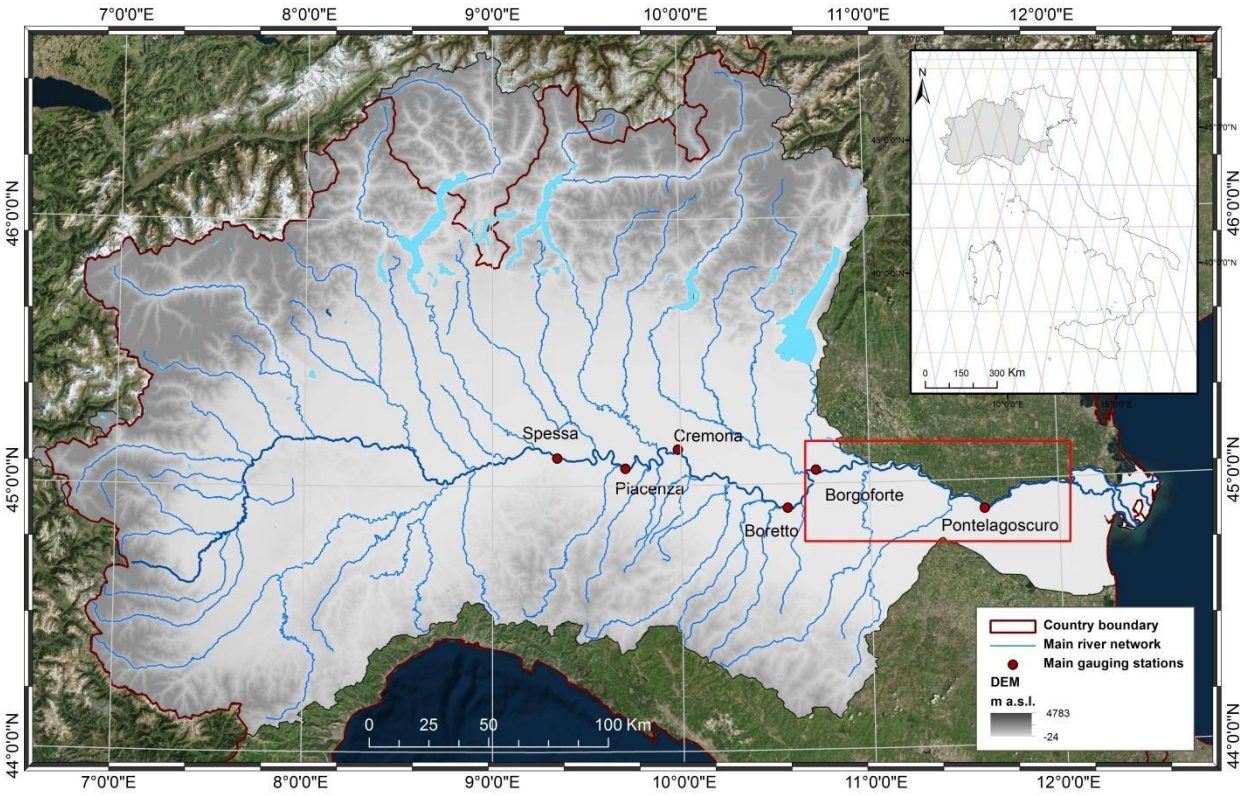

Figure 1. Po river basin with the main river network and principal gauging station; upper right box shows the SWOT nadir orbits over Italy, while the red box identifies the study area.

2.1 Data availability

In the light of the socio-economic importance of the Po Valley, the main river network is continuously monitored (see e.g., Montanari *et al.*, 2017). Red points in Figure 1 indicate some of the most important gauging stations along the river, where many hydrological variables (e.g. flow level, river flows, water turbidity, temperature, etc.) have been monitored and recorded since the 1920s, providing a robust and reliable knowledge of the hydrological and hydraulic regime of the river. In particular, daily average river flow data collected at the gauging station of Borgoforte (Figure 1) are used in this study for the identification of the hydraulic scenarios considered (Section 3.1).

River topography and bathymetry were obtained from a 2 m resolution digital elevation model (LiDAR and multi-beam sonar surveys performed by the Po River Basin Authority (AdB-Po) in 2005), which ensures an accurate reconstruction of the river morphology (see Castellarin *et al.*, 2011; Domeneghetti *et al.*, 2015).

Terrain elevations for the areas outside the embankment system have been extracted from the SRTM digital elevation model (Shuttle Radar Topography Mission, http://srtm.csi. cgiar.org). Given its limited spatial resolution (i.e., 90 m) and altimetric accuracy (errors in terms of ground elevation may vary from 4.7 m up to 9 m; see e.g. Rodriguez *et al.*, 2006; Schumann *et al.*, 2014; Domeneghetti, 2016), SRTM is only used for the topography description of the area outside the river system, and not relevant to the actual analysis.

2.2 SWOT coverage of the study area

The SWOT mission is planned to last at least 3 years, during which the satellite will provide continuous observations over almost all continental areas from 78°N to 78°S (Biancamaria *et al.*, 2016). The satellite has an orbit repeat period of nearly 21 days. At each overpass, the antennas will cover a 120 km swath, with a gap of 20 km at the orbit nadir.

Figure 2 shows the SWOT overpass over the study area, highlighting the left and right swaths sensed from the instrument (yellow areas) and the no-data nadir gap. Referring to this orbit, the present study considers three distinct, non-consecutive in time, overpasses over the study area, which are representative of three different hydrological conditions (see Section 3.1 for more details).

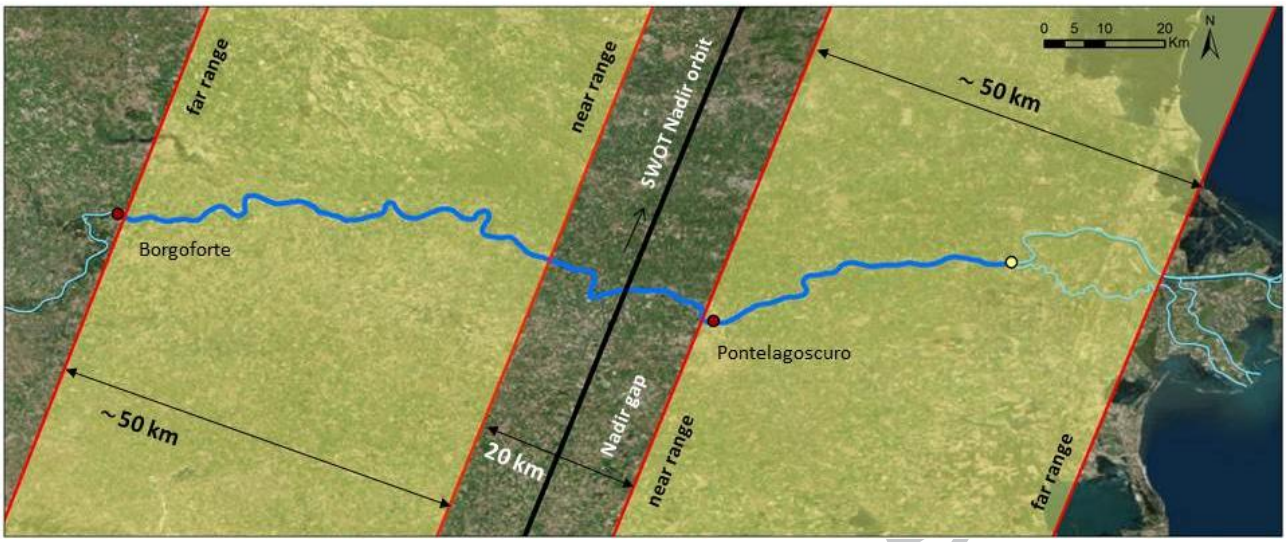

Figure 2. Example of a SWOT orbital pass over the study area: satellite swath (yellow areas), Po river reach considered in the study (dark blue; see also red box in Figure 1), flowing from the gauging station (red points) of Borgoforte to the beginning of the river delta (yellow point).

3 Pre-processing analysis

3.1 Hydrodynamic simulations of the Po River

This analysis considers three different flow scenarios that are representative of the possible river hydrological regime: high, low and mean flow conditions. Discharge values associated with those scenarios (Table 3) represent the upstream boundary conditions of the quasi-two-dimensional (quasi-2D) model implemented for the simulation of river dynamics. As in previous studies carried out on the same reach (see e.g. Castellarin *et al.*, 2009, 2011; Domeneghetti *et al.*, 2014, 2015) this work refers to a quasi-2D schematization of the river system, in which the interconnections between the main channel and dike-protected floodplains are reproduced through lateral structures that capture the real altimetric behavior of the minor embankments as detected by the LiDAR (Section 2.1). The reader is referred to those previous studies for more details on the model implementation, calibration and validation. Three distinct numerical simulations for high, low and mean flows have been run along the 140 km length river reach, imposing the uniform flow option at the downstream river section.

Table 3 summarizes some results of the hydraulic simulations and reports the variability in terms of width of the wetted river portion for the three cases. The high irregularity of the river topography induces a significant variation in water extent among the considered scenarios. The mean water extent may vary in time by a factor of three between low and high flow scenarios, while even higher variability can be observed at some specific locations (i.e. the largest flood extent is nearly 8 times the minimum for high and 4 times the minimum for low flows).

Figure 3 further highlights the river topography and the variability of the flood extent. Panel (a) refers to the high flow scenario and clearly shows the presence of lateral floodplains in the upstream part of the study area, which result in wetted areas much larger than those observed in the lower portion of the river. Panels (d), (e) and (f) in Figure 3 highlight the water level variability among the considered scenarios and clearly show the dimension of the embankment system, which may play a significant role when monitoring the river from satellites.

Table 3. Water extents for the considered hydraulic scenarios.

	Discharge *(m^3/s)*	***Max flow width*** *(m)*	***Mean flow width*** *(m)*	***Min flow width*** *(m)*
High flow	11 260	2472	805	306
Mean flow	1500	544	311	168
Low flow	170	458	258	109

3.2 Simulation data processing

A number of input data are required for the SWOT simulator to produce a realistic proxy of SWOT observations. As further detailed in Section 3.3, a high-resolution, high-accuracy terrain model (DTM) that incorporates river channel bathymetry and important hydraulic structures such as embankments and levees is needed. Also required is a 2D water depth grid that is associated with that terrain model. While a LiDAR-based DTM supplemented with SONAR batymetric profiles was readily available for this test case (see Section 2), a 2D water depth grid needed to be derived from the quasi-2D HEC-RAS output. The common procedure to transform the 1D or quasi-2D HEC-RAS simulation output, i.e. water surface elevation profiles, to an interpolated 2D gridded requires interpolation of the water elevations associated with all cross-sections to a regular gridded water height surface based on triangulation. The high-accuracy DTM can then be simply subtracted from this water surface grid to produce the desired water depth grid, which in this instance represented the input to the SWOT simulator along with the LiDAR DTM. The procedure adopted to reproduce the 2D water surface uses an interpolant based on the 2D Delaunay triangulation, which creates an irregular network where the surface always passes through the sample water elevation values imposed at the cross-section locations. A nearest neighbour interpolation is applied to create a regular grid based on this triangular irregular network (or TIN) surface.

The comparison of the "custom-generated" grid with 1D model output and water depth grid generated by other tools suitable for this task (i.e., HEC-GeoRAS) provides good results, with root mean square errors and bias of a few centimeters. Since this accuracy is comparable to that achieved during calibration of the HEC-RAS model with gauged water levels (see e.g., Castellarin *et al.*, 2010), we concluded that the performance of the "custom" translation of the HEC-RAS water surface profiles onto the 2D LiDAR grid is more than adequate for the purpose of this study. Also, it is worth highlighting that the 2D water surfaces need to

provide a realistic representation of the river under different conditions rather than its perfect representation. This said, the former represents the synthetic realities that the SWOT simulator will observe.

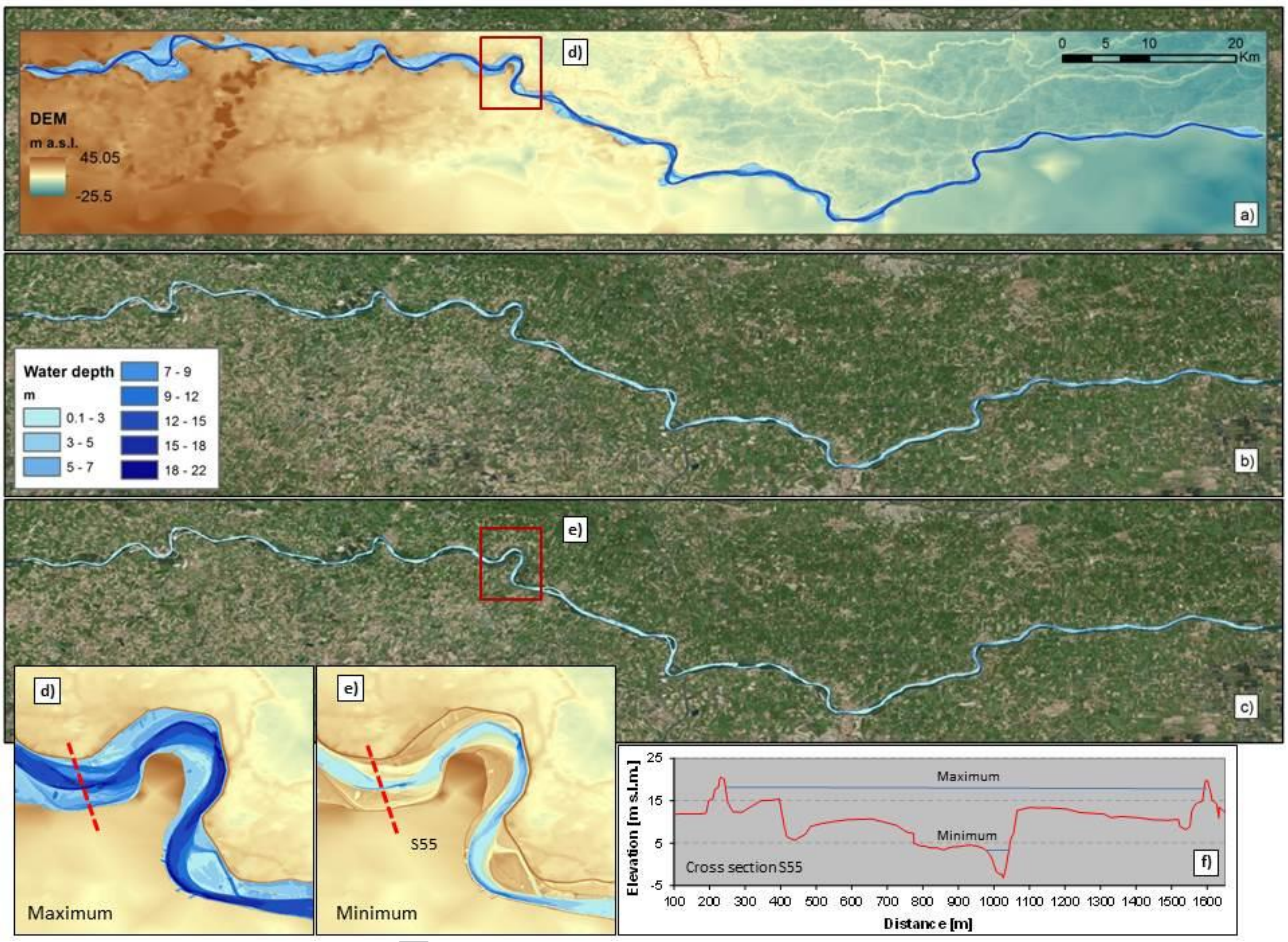

Figure 3. Input datasets for the SWOT simulator: 2D water depth coverage simulated for (a) high, (b) mean and (c) low river flow conditions (blue scale) and 2 m resolution DEM for river bathymetry and flood prone areas (from brown to green). Red boxes identify the same area used to show the different flood extents for (d) high and (e) low flow events, which may correspond to very different water depths at a given cross-section (e.g., cross-section S55; panel (f)).

3.3 SWOT Hydrology Simulator

The synthetic SWOT data for three overpasses were produced with the SWOT Hydrology Simulator developed by JPL. The simulator uses a high-resolution digital elevation model of the water surface and the terrain contained inside the study area to produce a simulated interferogram of the scene. Initially, the interferogram is produced in radar coordinates; it contains no noise and is only affected by terrain layover, a situation when radar returns from multiple targets reach the antennas at the same time, becoming indistinguishable and leading to height biases (Fjørtoft *et al.*, 2014). The presence of topographic elements that border the water surface (e.g. mountains or embankments) may determine the layover and affect the

observation accuracy. This interaction depends on the target position with respect to the satellite nadir (i.e., near or far range) and on the terrain slope, which should not be higher than the sensor look angle in order to prevent layover (0.6° or 3.9° for near and far range, respectively; Fjortfot *et al.*, 2014; Biancamaria *et al.*, 2016). Figure 4 provides a sketch of the terrain layover due to the presence of river embankments considering a sensing angle smaller than 30° (similar to the one adopted by SWOT; Fjortfot *et al.*, 2014) as for near-nadir viewing system, distinguishing different water extents (high and low flow), and two different river geometry configurations. Looking at Figure 4, it is evident how the river orientation and the presence of lateral floodplains influence the potential layover, which is expected to be more relevant when a river is parallel to the satellite orbit (Frasson *et al.*, 2017).

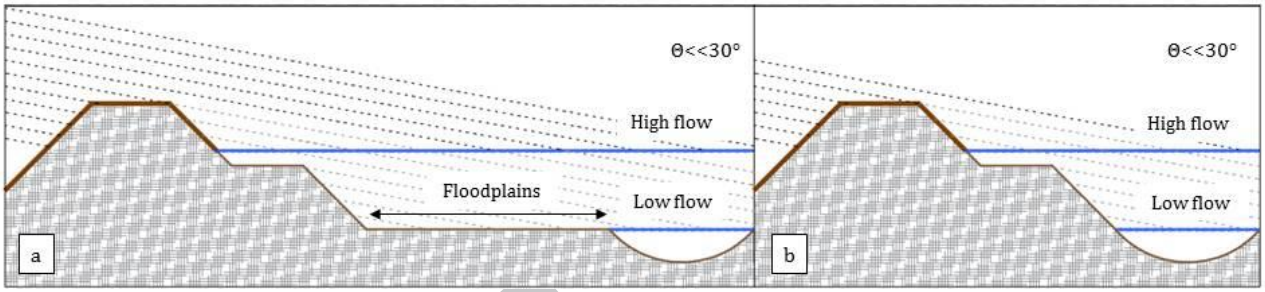

Figure 4. Layover illustration for embanked river in case of incidence angles <<30° and in case of (a) large or (b) absent lateral floodplains (modified from Fjortfot *et al.*, 2014). Dashed lines indicate constant range from the sensor; i.e. radar returns from the dashed line return to the sensor simultaneously.

The simulator uses a water mask to distinguish between land and water pixels and estimates the returned power from the targets according to the chosen land-water contrast. Ulaby and Dobson (1989) found Ka-band basckettering values, σ_0, ranging from −5 to −10 dB for different land surfaces (i.e., rock, soil, and vegetation) in case of a 0°–5° incidence range, observing also a slowly falling trend with increasing incidence angle. Moller and Esteban-Fernandez (2015) further investigated backscattered signals from water surfaces showing σ_0>10 dB for water bodies, even in case of limited wind speed. Fjortoft *et al.* (2014) found similar results and confirmed a difference in terms of Ka-band near-nadir backscattering coefficients of about 15 dB from land and water surfaces. In the light of these findings, we ran the simulation assuming a backscatter coefficient (σ_0) of -5 dB for land and 10 dB for water. These values appear robust and reliable based on most recent findings of measurement campaigns made with KaRIn instruments, however, further research and sensitivity analysis, out of scope of the present work, would provide additional insights on SWOT observation.

Next, the simulator mimics the expected performance of the SWOT systems by adding correlated circular Gaussian noise to the interferogram. The Gaussian noise correlation depends on geometric and signal-to-noise ratio decorrelations, which vary depending on whether the target contains water or land.

The Ka-band sensor will observe water bodies with a ground pixel resolution of nearly 6 m in the direction of the satellite, and from 60 m to 10 m (near and far range, respectively) in the direction perpendicular to the satellite track (Biancamaria *et al.*, 2010). Some spatial averaging is required to successfully geolocate the raw SWOT data, resulting in the definition of a pixel cloud, that is a collection of intrinsic pixels plotted with reference to a geographical coordinate system (i.e., WGS84) and holding information on the surface area and elevation. Radar returns from surface targets are in a quasi-regular grid with the aforementioned resolution when viewed in radar coordinates, i.e. range vs along-track position. However, after geolocation, a map of the target positions appears as a point cloud familiar to users of LiDAR data (Biancamaria *et al.*, 2016; Frasson *et al.*, 2017) when visualized in geographical coordinates. The distortions that prevent a 1:1 mapping from radar coordinates to geographical coordinates are due to topographic characteristics of the area (see Figure 4), as well as geolocation errors and possible distortions due to averaging procedures.

As in the planned SWOT processing procedure, the noisy interferograms and returned power images are smoothed through a process called "multi-looking", which averages the returned power of pixels found inside a window centered on the location of the target, reducing speckle at the cost of reduced spatial resolution [Cuchi, 1986; Ulaby *et al.*, 2014]. The number of pixels over which multi-look averaging is performed is an important mission design parameter. The current plan is to release several data products with various levels of multi-looking. Here, we examine the so-called "raw" data product, where only 4 pixels in the along-track and 4 pixels in the cross-track directions are averaged. This is valuable as it represents a bounding, worst case, scenario for water surface elevation error. The SWOT hydrology simulator currently does not include errors associated with a number of phenomena that will affect product accuracy, including dry and wet tropospheric path delays, ionospheric path delays, and spacecraft roll uncertainty.

According to the simulated multi-looked returned power, the simulator classifies targets into four groups: "land", "land near water", "water near land", "interior water". The first class contains land pixels with no water neighbors. The second class contains land pixels that have at least one neighbor classified as water.

The third class contains water pixels that have at least one neighbor classified as land. The last class contains water pixels that are completely surrounded by other water pixels (Frasson *et al.*, 2017).

The SWOT simulator uses the multi-looked interferograms for the generation of the geolocated pixel clouds and some of those simulated for this study are shown in Figures 6 and 7.

4 Methods

4.1 Water height error

Referring to objective (i), that is the evaluation of the accuracy on water height measurements expected from the satellite sensor, we first analyze, separately, the "raw" product (namely, pixel cloud) generated by the SWOT simulator for the three considered hydraulic scenarios (high, low and mean flow conditions). Considering each pixel at a time, independently of its classification, the values observed by the satellite are compared to the elevations extracted, at the same location, from the digital surface models (DSMs) used as input (section 3.2), which represent the river geometry and the "true" water surface elevation reproduced with the hydraulic model (see section 3.2). The elevation of the free surface, both for the wet or dry area, is evaluated as the average elevation over an area of 25 m x 25 m around the considered point. The error on water surface elevation, ε, is calculated for each simulated pixel as:

$$\varepsilon = h_{SWOT} - h_{Obs} \tag{1}$$

where h_{SWOT} and h_{Obs} represent the average free-surface values expected from SWOT and provided as synthetic input, respectively.

A second, finer analysis distinguishes among flooded and not flooded areas, thus considering only those points that are wet, or dry, in the synthetic simulations used as input for the simulator. Similarly, the same analysis is also performed distinguishing among the four pixel classifications described in section 3.3, thus evaluating the expected performances in relation to the nature of the observed surface (i.e. interior water, water near land edge, land near water edge and land).

4.2 Spatial variability

With reference to objective (ii) we investigate SWOT errors in relation to target distance from the satellite nadir track by evaluating the water height at different locations identified along the satellite overpass. Figure

5 shows a sketch of the river discretization adopted for the analysis. Starting from the satellite track (red line in Figure 5) the sensed swaths (left and right; see also Figure 2) are discretized by drawing lines parallel to the SWOT orbit spaced at 1 km along the river center line. In this study we refer to the surveyed river center line, but the Global River Width from Landsat (GRWL) database can also be used for applications on any target rivers (Allen and Pavelsky, 2015).

The intersections of the river center line with lines running in parallel to the satellite ground track represent the nodes (black points), which are considered representative of the averaging areas (i.e., pink area in Figure 5) and used to define the distance from the nadir. On average, each reference area covers a surface equal to 62 000 m^2, which corresponds to about the minimum extent of the water body for the science requirements (see Table 1). This said, it is worth highlighting here that science requirements (Rodriguez, 2015) specify the characteristics that the highest level of processed data (i.e., level-2 data product) should meet in terms of accuracy and resolution. However, those requirements are not given with respect to pixel clouds, which represent the basic unit of SWOT observation and which are considered in this study (see also Section 3.3). Reaching mission requirements stated in Table 1 will require the application of averaging procedures aimed at defining appropriate river stretches, which are still under definition (see also Frasson et al., 2017). Assuming these uncertainties and on-going research activities carried out within the mission team, this study is aimed at performing SWOT simulator to a real river topography under different flow conditions, providing additional insights on the value, potential and limitations of the future mission, rather than evaluating the achievement of the mission requirements. Although errors identified in this study are obtained by the averaging of multiple pixels, the methodology applied does not represent the one that will be applied to produce SWOT level-2 products. Thus, a direct comparison with mission requirements is not fair and may be misleading.

The study refers to each averaging area at a time and evaluates the mean error (ME) and the mean absolute error (MAE), for all the pixel points observed by the simulator and falling within the bounding area, distinguishing their classification (i.e., interior water, water near land edge, land near water edge, land).

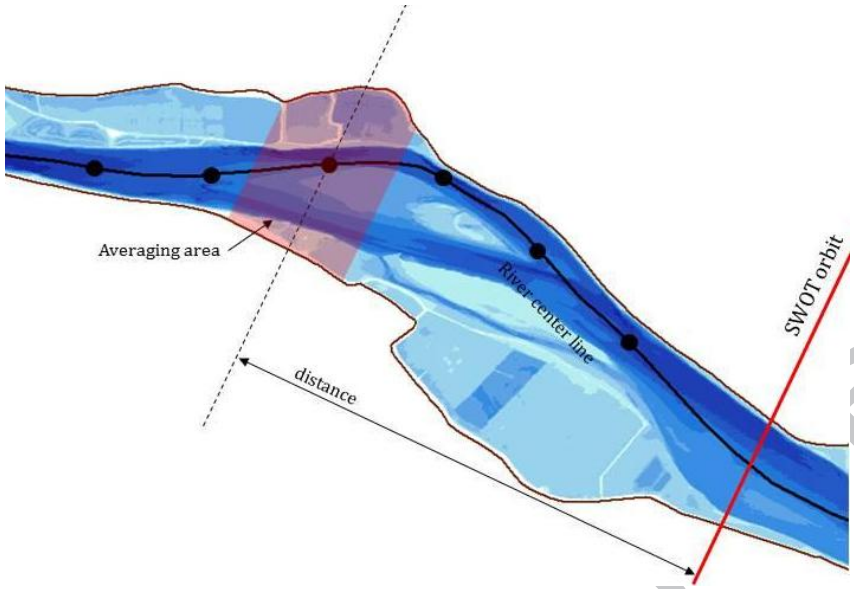

Figure 5. Schematic representation of the river discretization for the left swath; similar discretization has been adopted for the right swath.

5 Results and Discussion

5.1 Water height

Figure 6 shows the overall simulated observations expected from SWOT under different flows. The red line represents the satellite orbit over the Po river, while the dashed lines indicate the nadir gap (20 km width), where no interferometry measurements are available (see also Figure 2). Panels (a) and (b) show the pixel clouds that reproduce the surface elevation sensed for high and low flow conditions, respectively. Panels (c) and (d) provide a zoom-in of the same area and clearly highlight the variability of the sensed surface elevation showing heights detected from the radar considering all point classifications (land, land near water edge, water near land edge and interior water). Zoomed-in areas in panels (c) and (d) allow the identification of the expected single pixel cloud obtained from the satellite.

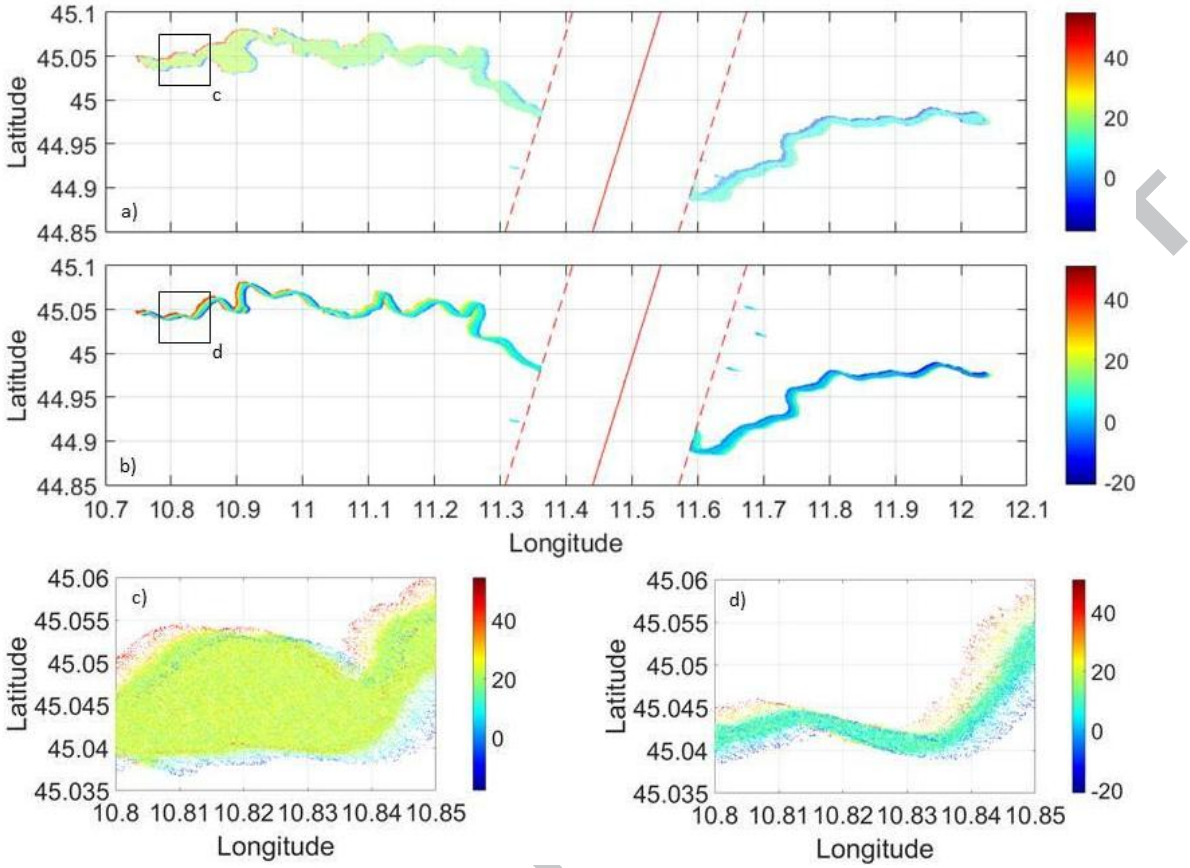

Figure 6. Pixel clouds showing the surface elevation (m a.s.l.) sensed by SWOT under different flow conditions, (a) high and (b) low flows, referring to all point classification; zoom in of panels (c) and (d) highlight the pixel clouds observed within a small river portion.

Despite the fact that the water surface extent is reasonably apparent in both cases, there are also obvious errors in the classification of wet and dry pixels: within the wetted area there are many pixels characterized by heights that are significantly different from the average water surface elevation. Also, boundaries along the water edge and the surrounding topography are not sharp, and points with low heights are mixed with others that seem to reproduce the embankment structure.

The position of the target area relative to the ground track (i.e. far or near range), as well as the river orientation and the slope of the surrounding topography (such as embankments) seem to lead to a spatial variability of the layover effects (Fjørtoft *et al.*, 2014). This appears evident in both panels (c) and (d) where the presence of the embankments affects the accuracy of water surface observations differently for the left and right river sides. These errors seem to occur along the overall swath, although the errors are larger at the near and far range. In addition, points affected by layover will likely be characterized by high geolocation

error since the vertical and horizontal accuracies are both functions of the phase interferogram accuracy (Biancamaria *et al.*, 2016).

In order to better evaluate the error on water heights, Figure 7 reports the water surface elevation only for those pixels classified as interior water by the simulator. This is motivated by the fact that those pixels are expected to be surrounded by other wet pixels and are also less likely to be affected by layover. For the same reasons, pixels classified as water near land edge may contain mixed return signals from both wet and dry areas and are also omitted. Water surface elevations shown on Figure 7 present a realistic reproduction illustration of all the considered scenarios (i.e., high, mean and low flows). The wetted areas appear more clearly identified in all the cases, and the decreasing elevation of the water surface moving from upstream to downstream appears realistic. Despite these promising performances, some unrealistic water surface values are present in all the simulations. Such pixels are particularly evident for the high flow scenario (upper panel of Figure 7) and especially in the proximity of the left embankment. Errors are more frequent at the near and far range of the satellite orbit, with the only exception being the upstream river reach (far range of the left swaths), where extremely high and low height values are recorded in all scenarios. The amount of error in the simulated pixels is surprisingly higher for the high flow event compared to mean and low flow scenarios. This may be explained by a greater impact from the layover effect induced by the proximity of the water surface to the main embankment system (see Figure 4). Referring, for example, to the river cross-section reported in Figure 3, the contiguity of the water with the embankment crest, as well as its riverside slope (close to 30-35%; see Fjørtoft *et al.*, 2014) and its orientation might accentuate the layover effect, producing biased observations in many cases. This would also explain why similar errors do not occur so frequently for lower flows, when the water surface is more distant from the surrounding structures.

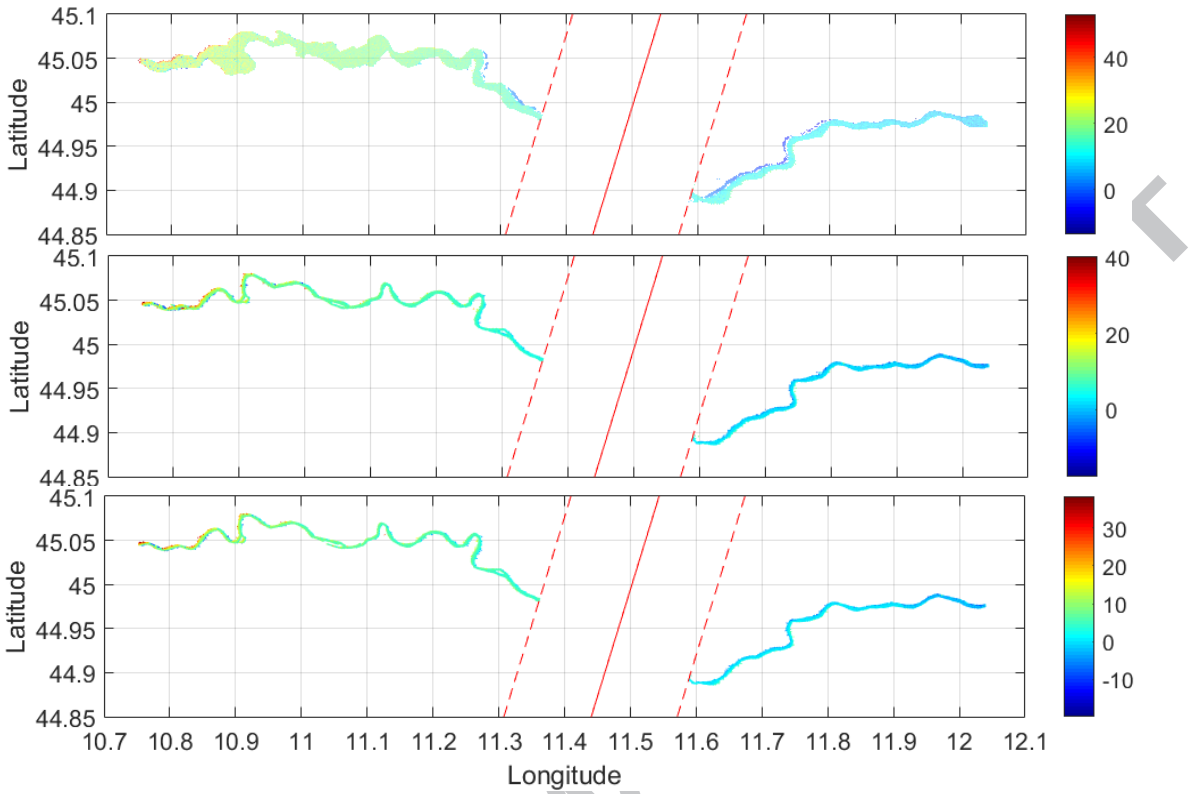

Figure 7. Pixel clouds reproducing the water surface elevation (m a.s.l.) for points classified as interior water under different flow conditions: high, mean and low flows (upper, intermediate and lower panel, respectively).

Table 4 reports mean errors (ME) and mean absolute errors (MAE) estimated for the overall swath assuming as reference areas the wet and dry extents taken from the input scenarios and considering all pixels that lie within.

As expected, Ka-band is less precise on estimating the land surface and errors are much larger for dry areas than for water bodies. For water bodies, errors are in general quite low and are smaller at lower flows than at higher flows. This is somehow counterintuitive, since the water body becomes smaller for low flows. However, the higher error associated with an extreme event can be explained by significant layover effects associated with the scenario in which the water reaches the embankment (see Figure 4 and 6). The higher the layover, the higher the geolocation errors, with many pixel points sensed as land that actually fall within wetted areas.

Table 4. Mean error (and mean absolute error; m) of water surface elevations estimated considering the overall extent of dry and wet areas as identified in the input scenarios.

	Dry area	Wet area
High flow	2.041 (6.79)	-0.111 (1.89)
Mean flow	-1.889 (7.15)	0.028 (2.58)
Low flow	-2.267 (7.17)	0.021 (2.57)

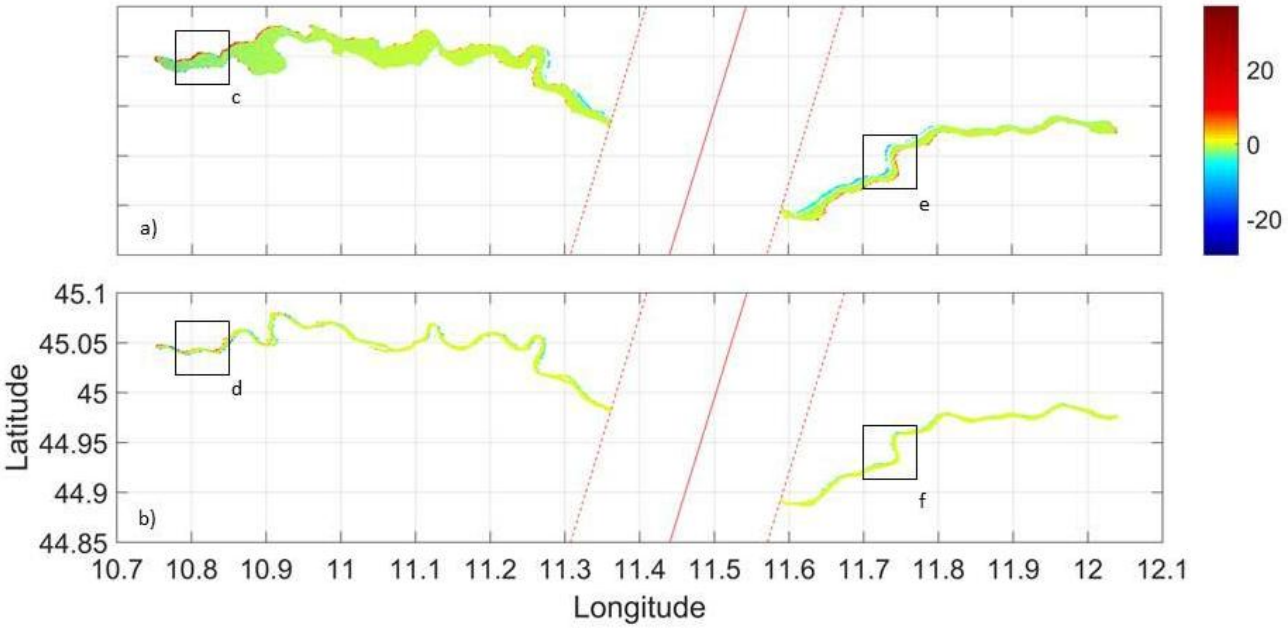

Figure 8. Errors (m) in water surface elevation sensed by SWOT at points classified as interior water under different flow conditions: (a) high and (b) low flows (panels (c), (d), (e) and (f) are reported in Figure 9).

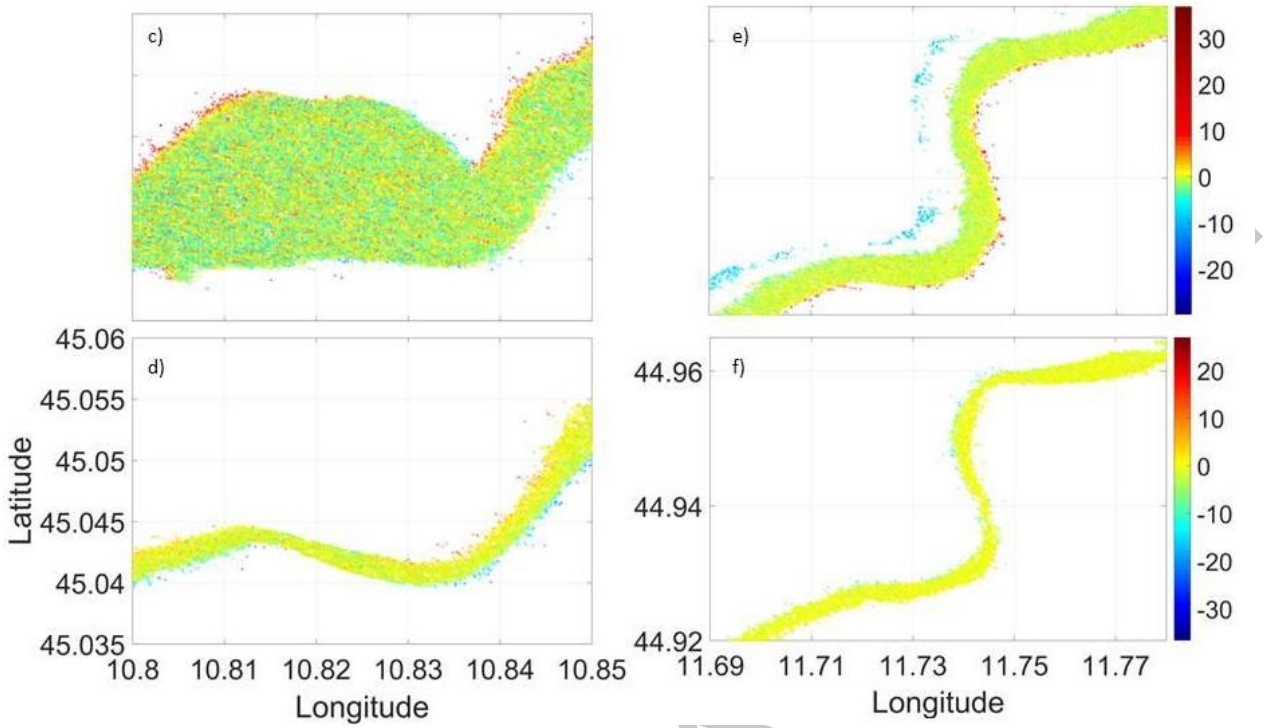

Figure 9. Errors (m) in water surface elevation at points classified as interior water under different flow condition: panels c) and e) refer to high flow, panels d) and f) refer to low flow (see boxes in Figure 8).

Figure 8 reports errors, ε (eq. (1)), on water surface elevation at each pixel cloud considering only interior water targets in case of high (a) and low (b) flow conditions. Figure 9 magnifies small regions shown in Figure 8, and it is apparent that many pixels have very small errors. At the same time, Figure 8 also highlights the presence of pixels with water heights very different from the real surface. Although some of those pixels are located in the middle of the wetted portion, the majority of the errors are located at water edges. Panels (c) and (e) highlight that overestimation typically occurs on the riverward edge of the embankment, becoming evident (errors as high as 15 m) when the orientation of the embankment system is aligned with the satellite track. Panels (d) and (f) confirm this behavior. In contrast, underestimation occurs on the landward side of the embankment, especially along the river reaches that flow parallel to the satellite orbit (see panels (e) and (d) in Figure 9).

Table 5 lists the mean error (and MAE) in surface elevation (both water and land) by distinguishing different point classifications provided by the simulator. Interior water outperforms all other classifications, and, as expected, the larger the water extent, the lower the error value for interior water, which ranges from an average value of 0.16 cm to -21.8 cm passing from high to low flow scenarios. Even though a direct comparison with the mission requirements is not appropriate, results for the interior water classification fall

within the error range expected for the smaller observable water extents (Table 1). Differently from what happens with a water body, the electromagnetic waves that reach non-water areas will be backscattered in all directions, and therefore less energy is returned to the satellite antenna. As a consequence, the sensing of land elevation is less efficient, with errors that reach almost half a meter for low flow. The detection of the boundary between land and water is even less precise, and sensing of water near land edge and land near water edge results in very large errors under all the considered flow conditions.

Table 5. Mean error (and mean absolute error; m) of surface elevations for different point classifications.

	Point classification				
	All points	Interior water	Water near land edge	Land near water edge	Land
High flow	0.040 (2.244)	-0.0016 (1.595)	0.378 (2.261)	0.773 (4.762)	0.059 (7.322)
Mean flow	-0.354 (3.498)	-0.157 (1.496)	-1.249 (2.323)	-1.489 (5.062)	-0.197 (7.377)
Low flow	-0.51 (3.64)	-0.218 (1.507)	-1.365 (2.421)	-1.588 (5.186)	-0.47 (7.22)

For the points classified as interior water and water near land edge, Figure 10 reports the histograms of errors on water surface elevation for all considered flows. The error distributions appear quite symmetric and not biased, with exceptions of water near land edge for mean and low flows, where the underestimation is prevalent.

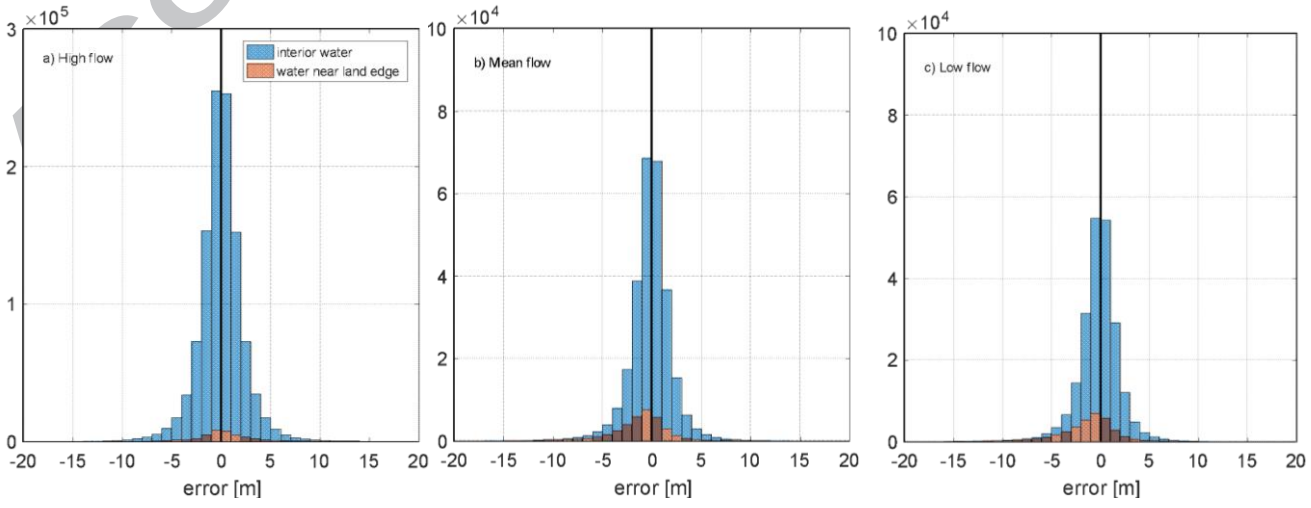

Figure 10. Histograms of errors, ε, on water surface elevation for the three scenarios considering points classified as interior water (blue bars) and water near land edge (brown bars).

5.2 Spatial variability of water height observations

Referring to the swath discretization described in Section 3.4.2 (see also Figure 5), Figure 11 shows the comparison among simulated and observed water surface profiles for the three considered scenarios using a ten-point moving average filter of pixel clouds classified as interior water. The adoption of a moving average filter of about 10 km is in line with the river stretch discretization suitable for SWOT product provision (Frasson *et al.*, 2017). Figure 11 shows a good performance in reproducing the water surface profile in case of high flow, while larger errors (i.e. underestimation) are expected for mean and low flows, especially at near and far range.

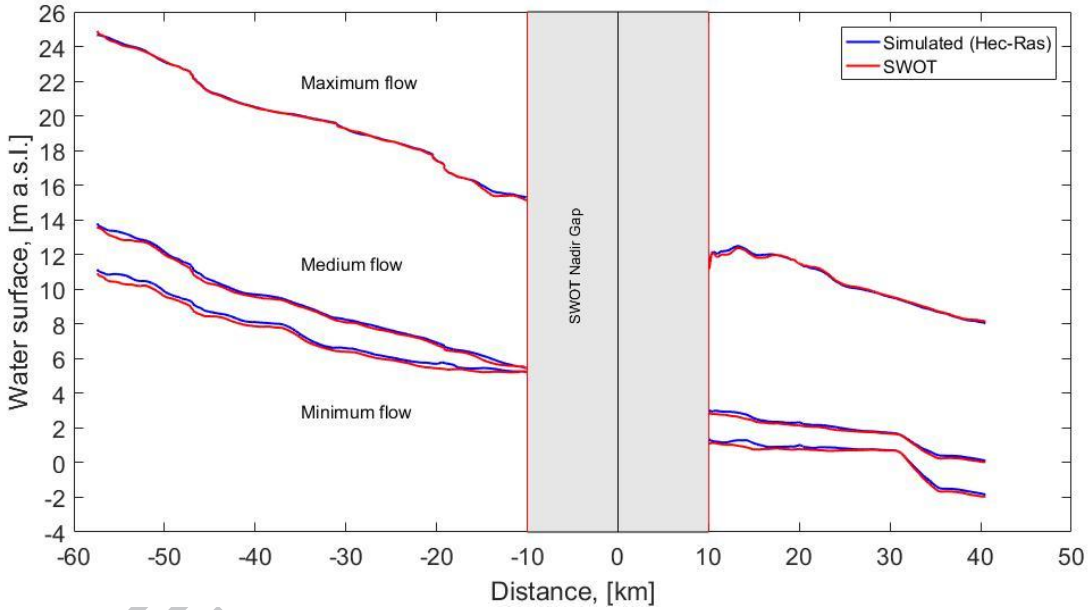

Figure 11. Water surface profiles for the three considered scenarios: (blue) Hec-Ras and (red) SWOT water profiles estimated considering an averaging area of 1 km^2 (see section 4.2) and a ten-point moving average filter.

Figure 12 reports the mean error (ME) calculated over each averaging area identified along the observed river stretch with a step of 1 km. Moving from the satellite track, panels in Figure 12 show the errors for pixel points classified as interior water (upper panel) and water near land edge (lower panel) for the three scenarios. For the points classified as interior water (upper panel of Figure 12), Figure 13 uses the same values and locates the errors along the river stretch in relation to their position and distance to the satellite track for the three events: upper, central and lower panel for high, mean and low flows, respectively.

For high flow condition (red points in Figure 12), errors on interior water are limited along the overall swath, with an average value equal to 0.072 m and a percentage of errors lower than ± 25 cm equal to 57%, 63%

and 60% for minimum, mean and maximum flow, respectively. Significant errors emerge at the border of the satellite swath (far range) where the overestimation is prevalent (see also Figure 9, panel c)). In contrast, near range areas underestimate the water surface (Figure 13, upper panel), especially on the right side where the unfavorable river orientation and the lower river width exacerbate the inaccuracies. Errors are generally small ($\varepsilon < \pm$ 25 cm) in the central part of the satellite swath, in particular in the range 20-45 km from the satellite track (in both directions), where the error is on average 0.012 m. High flow is, in general, associated with errors lower than that of other scenarios (upper panel of Figure 12), with the only exception of near range locations (from 10 to 20 km) where all simulations show limited accuracies and provide similar results. Errors of interior water points in case of mean and low flows (blue and black, respectively) are not biased and quite similar: average error equals -0.16 m for mean flow and -0.2 m for low flow. For both these scenarios the performance of the radar is limited at the far range locations, resulting in errors that may be larger than ± 50 cm. However, errors are smaller at the near range, where in both cases they are lower, if not comparable, to those observed for high flow condition.

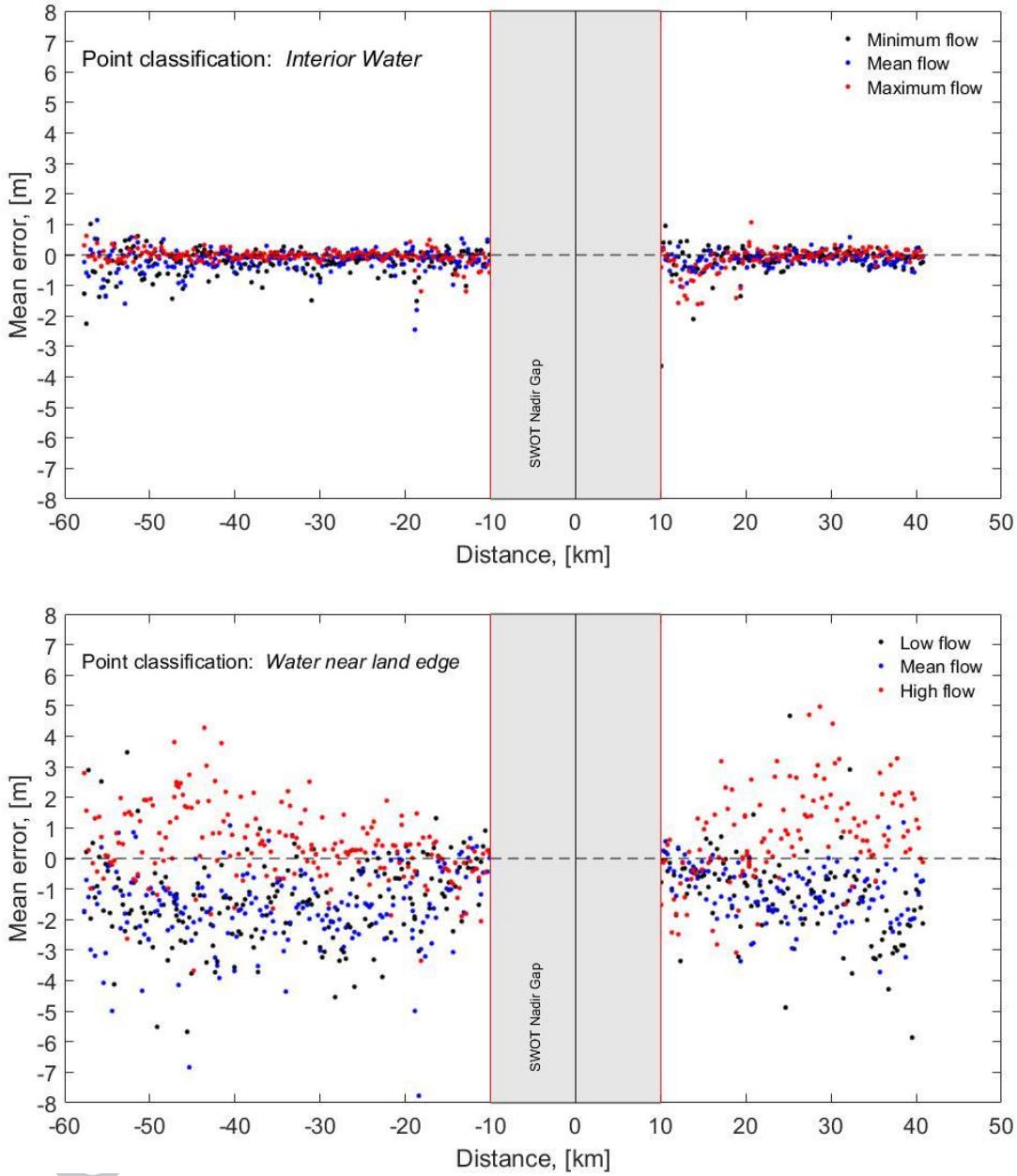

Figure 12. Mean error (ME) on water surface elevation for interior water (upper panel) and water near land edge (lower panel) points; points are shown in relation to the distance from the Nadir orbit (negative distances indicate the left swath).

In the upper panel of Figure 12 and panels of Figure 13, there are specific locations where the errors in water surface elevation are high, independent of the river flow conditions. These areas are particularly evident in the left swath at a distance of around 20 km from the satellite ground track, where all scenarios present high errors. Looking at the river geometry at this location, the influence of the river orientation is apparent, with high errors that occur when the main river, and thus the embankment system, is parallel to the satellite track. However, with the exception of the case above, the influence of the river orientation does not appear so obvious. Even though the river orientation alone does not appear sufficient to justify some errors, its

combination with the width of the water body and the layover induced by the surrounding topography may explain these errors (see Figure 4), especially significant in the near range of the left swath (see Figures 12 and 13, upper panels), with errors in case of high flow larger than those obtained for the other two scenarios. Panels of Figure 13 show the location of the ME of pixels classified as interior water. As expected, large errors are observed for all scenarios, with values up to a few meters, increasing from near range to far range. Different from previous results, the lower panel of Figure 12 shows some biases in all scenarios. Since these pixels have at least one neighbour point classified as land ("water near land edge"), these biases are related to the interaction with the surrounding terrain, which affects the backscattered signal. The different behavior observed in case of high flow is likely related to the terrain layover that masks the lower target (i.e., water surface) and provides overestimation (see also Frasson *et al.*, 2017). The occurrence of these biases for high flow events is more evident in the right swath than the left, and is probably due to the different river orientation, which makes the right swath more prone to terrain layover.

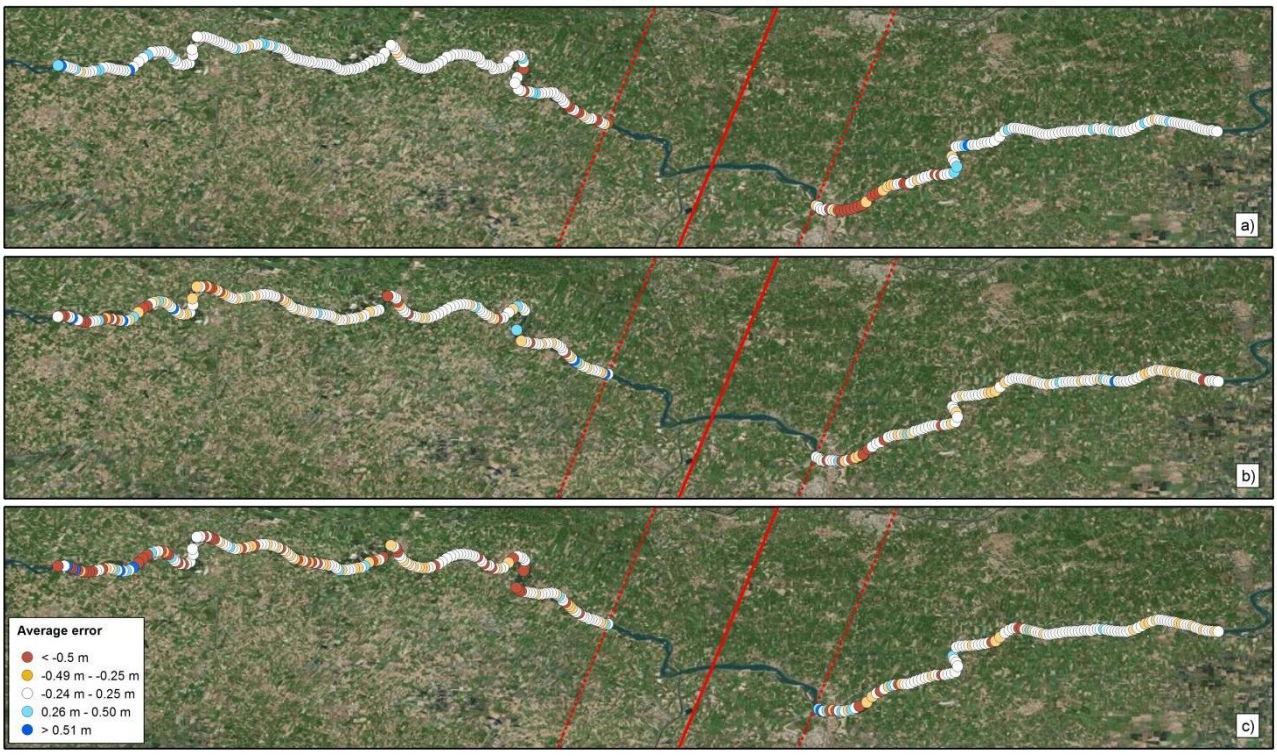

Figure 13. ME for all the points classified as interior water for (a) high , (b) mean and (c) low flow conditions.

6 Conclusion

This work evaluates the potential of the SWOT mission to accurately measure water surface elevations in rivers and provides additional insights concerning the performance of the satellite instrument under different flow conditions: high, low and mean flows. Satellite observations are modeled using the SWOT hydrology simulator over a ~140 km stretch of the Po river. The hydraulic conditions of the river are reproduced by means of a quasi-2D model built on high-accuracy topographic and bathymetric data, which allows investigation of the interaction of the radar signal with both water bodies and their surrounding topography.

The analysis highlights the high performances of the Ka-band radar interferometer on sensing the water bodies (i.e., interior water) with a mean error, in the worst case scenario, equal to -0.21 m using unprocessed ("raw") SWOT data (see Table 5). Although this study is not intended to directly verify the achievement of the mission requirements (the ultimate level of SWOT processed data are under definition), the results obtained represent a useful element of discussion that opens optimistic scenarios on the achievement of mission requirements. Because SWOT is not designed to accurately measure dry land, the identification of wet pixels located at the fringe of the wetted areas (i.e., water near land edge) is obviously quite inaccurate, with mean height errors exceeding 1 m in some cases (see Table 5). Errors for the high flow scenario are lower than those obtained for the other hydraulic conditions. Thus, as expected, the larger the water extent, the lower the error. Lower performances are expected for limited water extents, with the consequence that smaller rivers, or even low flow conditions in medium to large rivers, would be monitored with higher uncertainty. Unfortunately, these conditions (i.e., low flows and droughts) represent the most difficult hydrological regime to predict in case of absence of traditional observations (see e.g., Pugliese *et al.*, 2014; Castellarin *et al.*, 2013).

The study also shows that the river orientation and the target location relative to the satellite orbit (near and far range) affect the accuracy. In all the hydrological scenarios simulated, the better performances (lower errors) are normally observed in the central part of the swath, between 20 and 45 km from the satellite ground track. Even though the river orientation alone does not seem to compromise the observation, its combination with layover induced by the surrounding topography (e.g., embankment or other obstacles) may result in higher inaccuracies.

This work provides one of the few available detailed analyses to date of SWOT radar pixel accuracy over a real river case study using different flow conditions. Conclusions and insights were possible due to the application of the SWOT simulator, which enables a deeper understanding of the satellite's capabilities, and its potential applications, that cannot be inferred by referring, exclusively, to mission requirements or other "proxy" datasets. Despite using "raw", unprocessed, simulated satellite data, and thus neglecting the averaging process that will be performed before the final SWOT products are released, the results obtained in terms of water surface elevation are promising. Results of the present work provide useful insights into SWOT observations, helping the scientific community to become more familiar with observations that can be expected from the satellite and become aware of limitations and error sources. The findings are also valuable for further development of SWOT data products and for the identification of river reaches for which we can expect to have more reliable observations.

7 Acknowledgment

The authors are extremely grateful to the Interregional Agency for the Po River (AIPo) and Po River Basin Authority (AdBPo) allowing access to their high resolution DTM of River Po and GIS layers used in the analysis. G. Schumann's time on this work was partially funded under a SWOT Algorithm Development Team (ADT) service contract from the NASA/Caltech Jet Propulsion Laboratory. Data used for this work regarding the Po River are available upon request from the corresponding author (A. Domeneghetti: alessio.domeneghetti@unibo.it). Authors are also grateful to Editor, Associate Editor and two anonymous Reviewers for their meaningful comments.

References

Allen, G.H., Pavelsky, T.M., 2015. Patterns of river width and surface area revealed by the satellite-derived North American River Width data set. Geophys. Res. Lett. 42, 395–402. doi:10.1002/2014GL062764.

Alsdorf, D.E., Rodriguez, E., Lettenmaier, D.P., 2007. Measuring surface water from space. Rev. Geophys. 45, 1–24. doi:10.1029/2006RG000197.1.INTRODUCTION

Andreadis, K.M., Clark, E. a., Lettenmaier, D.P., Alsdorf, D.E., 2007. Prospects for river discharge and depth estimation through assimilation of swath-altimetry into a raster-based hydrodynamics model. Geophys. Res. Lett. 34, 1–5. doi:10.1029/2007GL029721

Andreadis, K.M., Schumann, G.J., 2014. Estimating the impact of satellite observations on the predictability of large-scale hydraulic models. Adv. Water Resour. 73, 44–54. doi:10.1016/j.advwatres.2014.06.006

Biancamaria, S., Andreadis, K.M., Durand, M., Clark, E.A., Rodriguez, E., Mognard, N.M., Alsdorf, D.E., Lettenmaier, D.P., Oudin, Y., 2010. Preliminary characterization of SWOT hydrology error budget and global capabilities. IEEE J. Sel. Top. Appl. Earth Obs. Remote Sens. 3, 6–19. doi:10.1109/JSTARS.2009.2034614

Biancamaria, S., Lettenmaier, D.P., Pavelsky, T.M., 2016. The SWOT Mission and Its Capabilities for Land Hydrology. Surv. Geophys. 37, 307–337. doi:10.1007/s10712-015-9346-y

Birkinshaw, S.J., O'Donnell, G.M., Moore, P., Kilsby, C.G., Fowler, H.J., Berry, P. a M., 2010. Using satellite altimetry data to augment flow estimation techniques on the Mekong River. Hydrol. Process. 24, 3811–3825. doi:10.1002/hyp.7811

Bonnema, M.G., Sikder, S., Hossain, F., Durand, M., Gleason, C.J., Bjerklie, D.M., 2016. Benchmarking wide swath altimetry-based river discharge estimation algorithms for the Ganges river system. Water Resour. Res. 52, 2439–2461. doi:10.1017/CBO9781107415324.004

Castellarin, A., Di Baldassarre, G., Brath, A., 2009. Floodplain managemente strategies for flood attenuation in the River Po. River Res. Appl.

Castellarin, A., Di Baldassarre, G., Brath, A., 2010. Floodplain management strategies for flood attenuation in the river Po. River Res. Appl. 27, 1037–1047. doi:10.1002/rra.1405

Castellarin, A., Domeneghetti, A., Brath, A., 2011. Identifying robust large-scale flood risk mitigation

strategies: A quasi-2D hydraulic model as a tool for the Po river. Phys. Chem. Earth, Parts A/B/C 36, 299–308. doi:10.1016/j.pce.2011.02.008

Domeneghetti, A., Castellarin, A., Brath, A., 2012. Assessing rating-curve uncertainty and its effects on hydraulic model calibration. Hydrol. Earth Syst. Sci. 16, 1191–1202. doi:10.5194/hess-16-1191-2012

Domeneghetti, A., 2016. On the use of SRTM and altimetry data for flood modeling in data-sparse regions. Water Resour. Res. 52, 2901–2918. doi:10.1002/2015WR017967

Domeneghetti, A., Carisi, F., Castellarin, A., Brath, A., 2015a. Evolution of Flood Risk Over Large Areas: Quantitative Assessment for The Po River. J. Hydrol. 527, 809–823. doi:10.1016/j.jhydrol.2015.05.043

Domeneghetti, A., Castellarin, A., Tarpanelli, A., Moramarco, T., 2015b. Investigating the uncertainty of satellite altimetry product for hydrodynamic modelling. Hydrol. Process. 29, 4908–4918. doi:10.1002/hyp.10507

Domeneghetti, A., Tarpanelli, A., Brocca, L., Barbetta, S., Moramarco, T., Castellarin, A., Brath, A., 2014. The use of remote sensing-derived water surface data for hydraulic model calibration. Remote Sens. Environ. 149, 130–141. doi:10.1016/j.rse.2014.04.007

Durand, M., Andreadis, K.M., Alsdorf, D.E., Lettenmaier, D.P., Moller, D., Wilson, M., 2008. Estimation of bathymetric depth and slope from data assimilation of swath altimetry into a hydrodynamic model. Geophys. Res. Lett. 35, 1–5. doi:10.1029/2008GL034150

Durand, M., Andreadis, K.M., Alsdorf, D.E., Lettenmaier, D.P., Moller, D., Wilson, M., 2008. Estimation of bathymetric depth and slope from data assimilation of swath altimetry into a hydrodynamic model. Geophys. Res. Lett. 35, 1–5. doi:10.1029/2008GL034150

Durand, B.M., Fu, L., Lettenmaier, D.P., Alsdorf, D.E., Rodriguez, E., Esteban-fernandez, D., 2010. The Surface Water and Ocean Topography Mission : Observing Terrestrial Surface Water and Oceanic Submesoscale Eddies. Proc. IEEE 98, 766–779.

Durand, M., Gleason, C.J., Garambois, P.A., Bjerklie, D., Smith, L.C., Roux, H., Rodriguez, E., Bates, P.D., Pavelsky, T.M., Monnier, J., Chen, X., Baldassarre, G. Di, Fiset, J.-M., Flipo, N., Frasson, R.P. d. M., Fulton, J., Goutal, N., Hossain, F., Humphries, E., Minear, J.T., Mukolwe, M.M., Neal, J.C., Ricci, S., Sanders, B.F., Schumann, G., Schubert, J.E., Vilmin, L., 2016. An intercomparison of remote sensing

river discharge estimation algorithms frommeasurements of river height, width, and slope. Water Resour. Res. 52, 4527–4549. doi:10.1002/2015WR018434.Received

Fjørtoft, R., Gaudin, J.M., Pourthié, N., Lalaurie, J.C., Mallet, A., Nouvel, J.F., Martinot-Lagarde, J., Oriot, H., Borderies, P., Ruiz, C., Daniel, S., 2014. KaRIn on SWOT: Characteristics of near-nadir Ka-band interferometric SAR imagery. IEEE Trans. Geosci. Remote Sens. 52, 2172–2185. doi:10.1109/TGRS.2013.2258402

Frasson, R.P. de M., Wei, R., Durand, M., Minear, J.T., Domeneghetti, A., Schumann, G., Williams, B.A., Rodriguez, E., Picamilh, C., Lion, C., Pavelsky, T., Garambois, P.-A., 2017. Automated River Reach Definition Strategies : Applications for. Water Resour. Res. 53, 8164–8186. doi:10.1002/2017WR020887

Getirana, A.C. V, 2010. Integrating spatial altimetry data into the automatic calibration of hydrological models. J. Hydrol. 387, 244–255. doi:10.1016/j.jhydrol.2010.04.013

Gleason, C.J., Hamdan, A.L.I.N., 2017. Crossing the (watershed) divide: satellite data and the changing politics of international river basins. Geogr. J. 2–15. doi:10.1111/geoj.12155

Hossain, F., Mazumder, L.C., Shahnewaz, S.M., Biancamaria, S., Lee, H., Shum, C.K., 2013. Proof of Concept of an Altimeter-Based River Forecasting System for Transboundary Flow Inside Bangladesh 587–601.

Jarihani, A.A., Larsen, J.R., Callow, J.N., McVicar, T.R. and Johansen, K. 2015. Where does all the water go? Partitioning water transmission losses in a data-sparse, multi-channel and low-gradient dryland river system using modelling and remote sensing. Journal of Hydrology. 529(3), 1511-1529, doi:10.1016/j.jhydrol.2015.08.030

Michailovsky, C.I., Milzow, C., Bauer-Gottwein, P., 2013. Assimilation of radar altimetry to a routing model of the Brahmaputra River. Water Resour. Res. 49, 4807–4816. doi:10.1002/wrcr.20345

Moller, D., Esteban-Fernandez, D., 2015. Near-nadir Ka-band field observations of freshwater bodies. Remote Sensing of the Terrestrial Water Cycle, Geophysical Monograph 206. First Edition. Edited by Venkat Lakshmi, John Wiley & Sons, Inc.

Montanari, A., Ceola, S., Baratti, E., Domeneghetti, A., Brath, A., 2017. Po River Basin, in: Singh, V.P.

(Ed.), Handbook of Applied Hydrology, Second Edition. McGraw Hill, pp. 116-1-4.

Pavelsky, T.M., Durand, M.T., Andreadis, K.M., Beighley, R.E., Paiva, R.C.D., Allen, G.H., Miller, Z.F., 2014. Assessing the potential global extent of SWOT river discharge observations. J. Hydrol. 519, 1516–1525. doi:10.1016/j.jhydrol.2014.08.044

Pena-Arancibia, J.L., Zhang, Y., Pagendam, D.E., Viney, N.R., Lerat, J., Dijk, A.I.J.M. Van, Vaze, J., Frost, A.J., 2015. Streamflow rating uncertainty: characterisation and impacts on model calibration and performance. Environ. Model. Softw. 63, 32–44. doi:10.1016/j.envsoft.2014.09.011

Prakash, C., Singh, V.P., 2016. Water balance, in: Singh, V.P. (Ed.), Handbook of Applied Hydrology, Second Edition. McGraw Hill, p. 3–1/11.

Pugliese, a., Castellarin, a., Brath, a., 2014. Geostatistical prediction of flow–duration curves in an index-flow framework. Hydrol. Earth Syst. Sci. 18, 3801–3816. doi:10.5194/hess-18-3801-2014

Rodriguez, E., 2015. Surface Water and Ocean Topography Mission Project, Science Requirements Document. JPL Doc. D-61923.

Rodriguez, E., Morris, C.C., Belz, J.J., 2006. A global assessment of the SRTM performance. Photogramm. Eng. Remote Sensing 72, 249–260. doi:10.14358/PERS.72.3.249

Schumann, G.J.-P., Andreadis, K.M., Bates, P.D., 2014. Downscaling coarse grid hydrodynamic model simulations over large domains. J. Hydrol. 508, 289–298. doi:10.1016/j.jhydrol.2013.08.051

Schumann, G.J.-P., Domeneghetti, A., 2016. Exploiting the proliferation of current and future satellite observations of rivers. Hydrol. Process. 30. doi:10.1002/hyp.10825

Shiklomanov, I.., Rodda, J.C., 2003. World water Ressources at the beginning of the 21st century. Press Cambridge University.

Singh, R.P., Gupta, P.K., 2016. Development in Remote Sensing Techniques for Hydrological Studies. Proc. Indian Natl. Sci. Acad. 82, 773–786. doi:10.16943/ptinsa/2016/48484

Smith, L.C., 1997. Satellite remote sensing of river inundation area, stage, and discharge: A review. Hydrol. Process. 11, 1427–1439. doi:10.1002/(sici)1099-1085(199708)11:10<1427::aid-hyp473>3.0.co;2-s

Smith, L.C., Pavelsky, T.M., 2008. Estimation of river discharge, propagation speed, and hydraulic geometry from space: Lena River, Siberia. Water Resour. Res. 44, n/a-n/a. doi:10.1029/2007WR006133

Sneddon, C., Fox, C., 2012. Water, Geopolitics, and Economic Development in the Conceptualization of a Region. Eurasian Geogr. Econ. 53, 143–160.

Solander, K.C., Reager, J.T., Famiglietti, J.S., 2016. How well will the SurfaceWater and Ocean Topography (SWOT) mission observe global reservoirs? Water Resour. Res. 52, 2123–2140. doi:10.1002/2015WR017952.

Tarpanelli, A., Barbetta, S., Brocca, L., Moramarco, T., 2013. River discharge estimation by using altimetry data and simplified flood Routing modeling. Remote Sens. 5, 4145–4162. doi:10.3390/rs5094145

Tomkins, K.M., 2014. Uncertainty in stream flow rating curves : methods , controls and consequences. Hydrol. Process. 464–481. doi:10.1002/hyp.9567

Tourian, M.J., Tarpanelli, A., Elmi, O., Qin, T., Brocca, L., Moramarco, T., Sneeuw, N., 2016. Spatiotemporal densification of river water level time series bymultimission satellite altimetry. Water Resour. Res. 52, 1140–1159. doi:10.1002/2015WR017654.

Tourian, M.J., Sneeuw, N., Bárdossy, a., 2013. A quantile function approach to discharge estimation from satellite altimetry (ENVISAT). Water Resour. Res. n/a-n/a. doi:10.1002/wrcr.20348

Ulaby, F.T., Dobson, M.C., 1989. Handbook of Radar Scattering Statistics for Terrain. Boston, MA, USA: Artech House, 1989.

Vörösmarty, C., Askew, A., Grabs, W., Barry, R.G., Birkett, C., Döll, P., Goodison, B., 2001. Global Water Data : A Newly Endangered Species. Eos (Washington. DC). 82, 54–58.

Wilson, M.D., Durand, M., Jung, H.C., Alsdorf, D., 2015. Swath-altimetry measurements of the main stem Amazon River: Measurement errors and hydraulic implications. Hydrol. Earth Syst. Sci. 19, 1943–1959. doi:10.5194/hess-19-1943-2015

Wolf, A.T., Natharius, J.A., Danielson, J.J., Ward, B.S., Pender, J.K., 1999. International river basins of the world. International Journal of Water Resources Development, 15(4), 387– 427. https://doi.org/10.1080/07900629948682